TOPICAL REVIEW — Quantum information

Disorder and decoherence in coined quantum walks*

Zhang Rong(张 融)[a], Qin Hao(秦 豪)[a], Tang Bao(唐 宝)[a], and Xue Peng(薛 鹏)[a,b]†

[a] Department of Physics, Southeast University, Nanjing 211189, China
[b] State Key Laboratory of Precision Spectroscopy, East China Normal University, Shanghai 200062, China

(Received 8 October 2013)

This article aims to provide a review on quantum walks. Starting form a basic idea of discrete-time quantum walks, we will review the impact of disorder and decoherence on the properties of quantum walks. The evolution of the standard quantum walks is deterministic and disorder introduces randomness to the whole system and change interference pattern leading to the localization effect. Whereas, decoherence plays the role of transmitting quantum walks to classical random walks.

Keywords: quantum walk, disorder, decoherence

PACS: 03.67.Ac, 42.50.Pq, 74.50.+r **DOI:** 10.1088/1674-1056/22/11/110312

1. Introduction

The discovery of quantum mechanics has revealed counter-intuitive character of the nature. The quantum effects which are unimaginable in classical world have been studied and the applications of the quantum effects on technology have been exploited. In recent years, quantum information theory has been brought forward with the hope of design of powerful devise, such as quantum computation. We will introduce one of many aspects of quantum information: quantum walks (QWs), the quantum version of random walks (RWs). We focus on the studies of the non-classical properties of QWs induced by disorder or decoherence in this review.

QWs were used to study the dynamics of quantum diffusion originally in 1960's.[1] Aharonov presented QWs with quantum optical applications in mind in 1993.[2] In recent years, QWs attracted much interest in the context of quantum computation and quantum communication. Motivated by application of QWs for quantum algorithm, the continuous-time QWs and discrete-time QWs have been studied. We focus on the research literatures on the discrete-time QWs. The properties and applications of continuous-time QWs were shown in a review article.[3]

Based on the non-classical properties, QWs can be used to devise new quantum algorithms,[4–7] which exponentially speed up compared with the algorithms based on RWs. Furthermore, QWs can be used to implement universal quantum computing[8–11] and perfect state transfer.[12] QWs can also be used to model and study biological phenomenon, such as the energy transfer in photosynthesis,[13] and other complex phenomenon, such as Anderson localization[14,15] and topological phases.[16,17] The model of QWs also makes connections with the field of quantum chaos.

In this review, we will firstly overview the pure QWs without disorder and decoherence (we call standard QWs in the following) in the Section 2. Then, we introduce the non-classical effect of the localization in QWs induced by disorder in Section 3 and the impact of decoherence on QWs[18–22] will be discussed in Section 4. Finally, QWs with disorder and decoherence realized experimentally through photons in bulk optical system, waveguide, and fiber are shown in Section 5.

2. Standard coined discrete-time QWs

In this section, we describe the standard QWs in a discrete position space with discrete time evolution. We start with the simplest example of one-dimension (1D) QWs on the line. In the simple case of 1D QWs on the line, we set up notions of QWs and introduce the methods of solution. Moreover, different properties between RWs and QWs are exhibited apparently, such as the increased spreading velocity of the quantum walker. Then, the extended QWs in higher dimensions with multi-coins are introduced briefly.

We recall the RWs and then introduce the quantum counterpart of it. The walker moves on the line with a two-side coin. He tosses the coins first, then moves one step to the right if the coin is head or one step to the left if the coin is tail. The walker repeated such process many times, and the probability distribution is binomial. After t steps, the standard deviation of position σ is $\sqrt{t}$, and the walker spreads on average $\sqrt{t}$ away from the origin.

*Project supported by the National Natural Science Foundation of China (Grant Nos. 11004029 and 11174052), the Natural Science Foundation of Jiangsu Province, China (Grant No. BK2010422), the Ph.D. Program of the Ministry of Education of China, the Excellent Young Teachers Program of Southeast University of China, the National Basic Research Program of China (Grant No. 2011CB921203), and the Open Fund from the State Key Laboratory of Precision Spectroscopy of East China Normal University.

†Corresponding author. E-mail: gnep.eux@gmail.com

© 2013 Chinese Physical Society and IOP Publishing Ltd

2.1. One-dimensional standard QWs

We take the example from Ref. [2] to illustrate the term of QWs. Assume the state of a quantum particle on a line is described by the wave function ψ_{x_0} which corresponds to a wave-package localized around the position x_0. The shift of the particle corresponding to the step of length l is depicted by the unitary operator $U_l = \mathrm{e}^{-\mathrm{i}pl/\hbar}$, and $U_l|\psi_{x0}\rangle = |\psi_{(x_0-l)}\rangle$, where p is the momentum operator. Assume the quantum particle has another freedom degree: spin-$\frac{1}{2}$. The operator of z component of spin is represented by S_z, the two eigenstates satisfy $S_z|\uparrow\rangle = \frac{\hbar}{2}|\uparrow\rangle$ and $S_z|\downarrow\rangle = -\frac{\hbar}{2}|\downarrow\rangle$, and the states $|\uparrow\rangle$ and $|\downarrow\rangle$ correspond to spin-up and spin-down state in spin space, respectively. For simplicity, we set $\hbar = 1$ in the following part. The state of the spin-$\frac{1}{2}$ particle is usually described by a vector with two components $|\varphi\rangle = (|\uparrow\rangle, |\downarrow\rangle)$, where normalization $\langle\uparrow|\uparrow\rangle^2 + \langle\downarrow|\downarrow\rangle^2 = 1$ is satisfied. We can express the state of the particle in another form by considering two freedom degrees of spin and position of the quantum particle as: $|\varphi\rangle = c_\mathrm{a}|\uparrow\rangle \otimes |\varphi\rangle_\uparrow + c_\mathrm{b}|\downarrow\rangle \otimes |\varphi\rangle_\downarrow$, where two wave functions satisfy $\langle\varphi_\uparrow|\varphi_\uparrow\rangle = \langle\varphi_\downarrow|\varphi_\downarrow\rangle = 1$, so that $|c_\mathrm{a}|^2 + |c_\mathrm{b}|^2 = 1$. The conditional shift operator of the particle can be expressed as the unitary operator $U_\mathrm{s} = \exp(-2\mathrm{i}S_z \otimes pl)$ which makes the particle move $-l$ or l along the line in position space, depending on the spin state. For example, if the particle is initially in the spin-up state $|\uparrow\rangle \otimes |\varphi\rangle^\uparrow_{x_0}$, it will be shifted to the left l $|\uparrow\rangle \otimes |\varphi\rangle^\uparrow_{x_0-l}$, and in the spin-down state $|\downarrow\rangle \otimes |\varphi\rangle^\downarrow_{x_0}$, it will be shifted to the right l $|\downarrow\rangle \otimes |\varphi\rangle^\downarrow_{x_0+l}$. This is similar to the moving of a walker with a coin: with head the walker moves to right and with tail the walker moves to left. If the initial state is in the superposition state $|\Psi_0\rangle = (a|\uparrow\rangle + b|\downarrow\rangle) \otimes |\varphi\rangle_{x_0}$ with $|a|^2 + |b|^2 = 1$, after the operation of the conditional shift operation, we can obtain the superposition of position states $|\Psi\rangle = U|\Psi_0\rangle = a|\uparrow\rangle \otimes |\varphi\rangle^\uparrow_{x_0-l} + b|\downarrow\rangle \otimes |\varphi\rangle^\downarrow_{x_0+l}$. It is the superposition of different positions that lead to different properties of QWs from those of RWs. Because the spin operator S_z is expressed as $S_z = \frac{1}{2}(|\uparrow\rangle\langle\uparrow| - |\downarrow\rangle\langle\downarrow|)$, we have

$$U_\mathrm{s} = \mathrm{e}^{-\mathrm{i}(|\uparrow\rangle\langle\uparrow| - |\downarrow\rangle\langle\downarrow|)\otimes pl}. \tag{1}$$

The rotation of the spin can be expressed as

$$C = \begin{pmatrix} \cos\theta & -\sin\theta \\ \sin\theta & \cos\theta \end{pmatrix}. \tag{2}$$

QWs are realized by repeating the succession of the rotation operation shown in Eq. (2) and the conditional shift operator in Eq. (1).

In the above example, two freedom degrees are spin and position, usually the spin rotation is considered as the toss of a quantum coin. Actually, in the physical realization, one can choose other freedom degrees, such as polarization of photon and photon number, or atomic energy and position. We will generalize the example mentioned above with one of the freedom degrees corresponding to the coin and the other corresponding to the walker. The standard 1D coined QWs consist of a quantum coin and a quantum walker. The quantum walker tosses a two-state quantum coin, then moves one step to right or left according to the state of the quantum coin. The Hilbert space of the whole system is a tensor product of two Hilbert space $\mathcal{H}_\mathrm{c} \otimes \mathcal{H}_\mathrm{w}$, where $\mathcal{H}_\mathrm{c}$ is spanned by two states of the coin $|c\rangle$ with $c = 0, 1$, and $\mathcal{H}_\mathrm{w}$ is spanned by the vectors $|x\rangle$ ($x \in \mathbb{Z}$), which is the position of the walker on the 1D chain. In one step of the evolution, we first flip the coin, then shift the walker according to the state of the coin. The unitary operator which describes the evolution is

$$U = \left(\sum_c |c\rangle\langle c| \otimes S_\mathrm{c}\right)(C \otimes I), \tag{3}$$

where C is the coin flipping operator which is unitary and equivalent to the rotation operator given by Eq. (2). For $\theta = \pi/4$, the operator C is known as the Hadamard operator given by

$$H = \frac{1}{\sqrt{2}}\begin{pmatrix} 1 & 1 \\ 1 & -1 \end{pmatrix}. \tag{4}$$

The I is the identity operator on the walker, and S_c is the shift operator which plays the similar role of the conditional shift operator mentioned in Eq. (1), $S_\mathrm{c}|x\rangle = |x + (-1)^c\rangle$ $(c = 0, 1)$. Without loss of generality, we assume the walker initially in the position $x = 0$ and the state of coin in the superposition of $|\uparrow\rangle$ and $|\downarrow\rangle$. Therefore, the initial state of the whole system is

$$\Psi(0) = (a|\uparrow\rangle + b|\downarrow\rangle)_\mathrm{c} \otimes |0\rangle_w. \tag{5}$$

After t steps, the final state is

$$\Psi(t) = U^t\Psi(0). \tag{6}$$

If we measure the coin state in the standard basis $|\uparrow\rangle$ and $|\downarrow\rangle$ after each step, the interference between different positions will be destroyed totally, and we will obtain the classical RWs. While in QWs, the unitary operator U is applied repeatedly without measurement, and thus the correlations between different positions are kept and interference exists in subsequent steps.

The 1D QWs on the line are solved rigorously in many ways, such as path counting, Fourier transformation,[23] and the algebra of the matrix.[24,25] Thus, the properties of QWs can be obtained through the solution. Usually, the position distribution $P(x,t)$ and the standard deviation σ (or variance σ^2) are used to represent the properties of QWs. $P(x,t)$ shows the probabilities of the walker at each position x after t steps of evolution, and $P(x,t)$ is obtained by tracing out the coin and calculating the square modulus of the wavefunction of the walker. The standard deviation $\sigma = \sqrt{\langle x^2\rangle - \langle x\rangle^2}$ quantifies the velocity of the walker spreading away from the origin.

The initial state of the coin have effects on each step of the QW evolution, so the distributions depend on the initial coin state. The distribution is symmetric if the initial coin state is

$(|0\rangle + \mathrm{i}|1\rangle)/\sqrt{2}$. The simulation result of the distribution for 1D QWs (blue line) and for RMs (red line) are shown in Fig. 1. The quantum walker appears at the distance $\propto t$ away from the origin after t steps and the position distributions are nearly uniform in the range $\left[-t/\sqrt{2}, t/\sqrt{2}\right]$. While for classical RWs, the walker runs away from the origin $x = 0$ to the distance $\propto \sqrt{t}$ with exponentially small probability after t steps. Thus, 1D QWs spreads quadratically faster than RWs.

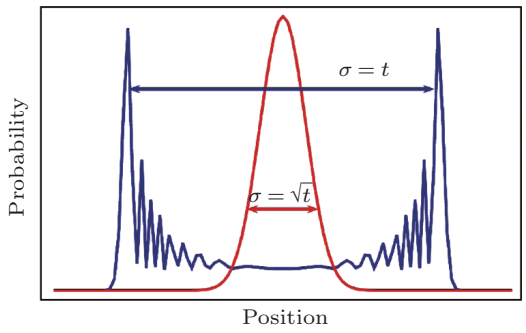


Fig. 1. The position distributions of QWs (blue line) and RWs (red line).

2.2. High-dimensional QWs

QWs can be extended to high-dimensional (d-dimensional with $d \geqslant 2$) with generalizations of 2^d-dimensional coin operator and generalized conditional shift operator which makes the walker move in d-dimension space. The generalized coin toss operator can be expressed in a separable way by the tensor of Hadamard coin tossing as

$$C_d = H \otimes H \otimes \cdots \otimes H, \tag{7}$$

where H is the Hadamard operator. The generalized coin operator have another non-separable form: the discrete Fourier transform (DFT) coin operator and Grover coin operator. DFT coin operator C_{DFT} is defined in the 2^d-dimensional basis $|\mu\rangle$ ($\mu = 0, 1, \ldots, 2^d - 1$), which transforms any eigenstate to an equally weighted superposition of all the eigenstates,

$$C_{\mathrm{DFT}}|\mu\rangle = \frac{1}{\sqrt{2^d}} \sum_{\nu=0}^{2^d-1} \mathrm{e}^{2\pi\mu\nu/2^d}|\nu\rangle. \tag{8}$$

The DFT operator can entangle different positions of the walker. The Grover coin operator C_{G} is defined in the same basis used above,

$$C_{\mathrm{G}}|\mu\rangle = \frac{1}{\sqrt{2^d}} \left(-2|\mu\rangle + \sum_{\nu=0}^{2^d-1} |\nu\rangle \right). \tag{9}$$

The analytical solution of high-dimensional QWs can only be obtained for special graph with fixed degree and high symmetry.[26] The high-dimensional QWs with separable internal transformation exhibit faster spreading compared with 1D QWs as shown in Fig. 2.[27] The standard deviations of 2D and 3D QWs grow linearly with time, however, the slopes for 2D and 3D QWs are bigger than that for 1D QWs. The standard deviation with DFT coin tossing operator which is non-separable transformations is also linear with time as shown in Fig. 3, but the slope is less than that with separable coin operator. If another non-separable Grover coin tossing operator is chosen, the velocity of the walker is suppressed and the walker is nearly localized at the origin as shown in Fig. 4. Thus, the spreading velocity of the walker in high dimension is reduced by the entanglement between the spatial degrees of freedom.

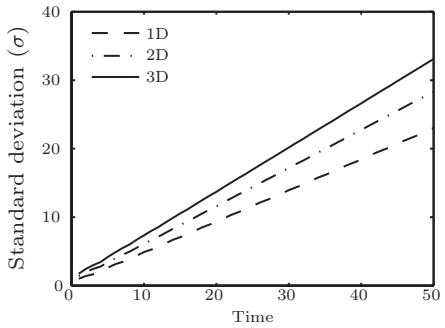


Fig. 2. Time dependence of standard deviation for the tensor of Hadamard coin flipping.[27]

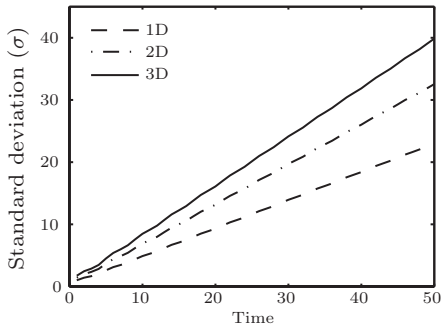


Fig. 3. Time dependence of standard deviation for the DFT coin operator.[27]

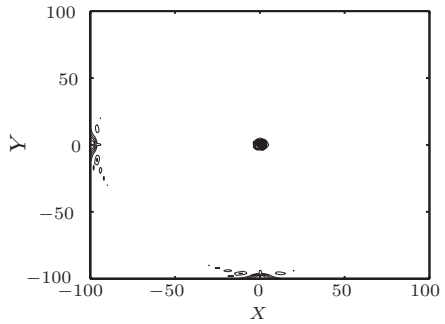


Fig. 4. Probability distribution of the 2D QWs with the Grover coin operator.[27]

Aside from the theoretical research literatures on QWs, QWs have been realized and non-classical effects of QWs have been verified experimentally in energies of the NMR system,[28–30] trapped ions,[31,32] and trapped neutral atoms,[33,34] photons in beam splitter array,[35–37] fibers,[38–41] and laser-writing waveguides.[42,43] In real experiments, the impacts from the environment and the decay of the quantum

system always exist, which can induce disorder and decoherence in QWs. Thus, many research literatures focus on the properties and applications of QWs with disorder and decoherence.

3. Simulation of Anderson localization in a QW architecture

Firstly, we focus on the properties of QWs with disorder. Unlike RWs, the evolution of the standard QWs is deterministic, whereas disorder introduces randomness to the whole system and leads to the change of interference pattern. Thus, the periodicity dynamics of the whole system is broken by disorder and localization effect can be observed. The prediction that the wave function of the particle in a static disordered medium becomes localized has been given based on the transport of electrons in disordered crystal by Anderson in 1958.[44] Thus, we call such phenomenon Anderson localization. Anderson localization arises from destructive interference among scattering paths of a propagating quantum particle, and results in the absence of diffusion. It has been experimentally investigated in different physical systems. In this section, Anderson localization of QWs with different kinds of disorders added on the walker are discussed in Section 3.1 and disorders on the coin in Section 3.2. Localization effect for QWs with different kinds of disorders can be explained analytically by the method mentioned in Ref. [45]. We will introduce the method in detail by the example of 1D QWs with phase disorder at the origin position of the walker.

3.1. QWs with disorder on the position space of the walker

We start with a simple case of 1D QWs with a single phase defect at the origin position of the walker.[45] The translational symmetry of the model is modified by the phase disorder $\phi \in (0, 2\pi)$ whenever the walker is at the position $x = 0$. In this situation, the unitary operator for one step evolution is modified compared with that of the standard 1D QWs,

$$U_\phi = \left(\sum_c |c\rangle\langle c| \otimes S_c^\phi \right) (H \otimes I), \tag{10}$$

where $S_c^\phi |x\rangle = \mathrm{e}^{\mathrm{i}\phi\delta_{x,0}} |x + (-1)^c\rangle$ $(c = 0, 1)$ and $\delta_{x,0}$ is the Kronecker δ. The state of the whole system is written as

$$|\Psi\rangle = \sum_x (\alpha_x |0\rangle|x\rangle + \beta_x |1\rangle|x\rangle), \tag{11}$$

where x is the position of the walker, and α_x and β_x are the amplitudes of the coin states $|0\rangle$ and $|1\rangle$, respectively. The walker is assumed at the origin position $x = 0$ initially without loss of generality. The model of 1D QWs with phase disorder at origin can be solved analytically. The non-classical properties of are studied and the localization effect is explained below.

The position distributions of 1D Hadamard QWs with a single phase disorder $\phi = \pi/3$ at $x = 0$ after 50-step evolution are shown in Fig. 5 by choosing symmetric $|\psi_0^+\rangle = (|0\rangle + \mathrm{i}|1\rangle)/\sqrt{2}$ and antisymmetric $|\psi_0^-\rangle = (|0\rangle - \mathrm{i}|1\rangle)/\sqrt{2}$ initial coin states. With disorder $\phi = \pi/3$ at $x = 0$, there is localization effect in the position $x = 0$ observed for the antisymmetric initial coin state $|\psi_0^-\rangle$ and the probability of the walker in $x = 0$ is about 0.3, while for the symmetric initial coin states $|\psi_0^+\rangle$ no localization effect is observed. Thus, the example mentioned above shows that localization effect depends on the initial coin state. The walk behave localization if the probability of the certain position does not tend to 0 in the limit of infinite time. Numerical calculations show that in 1D QWs with static disorder at origin the walker shows localization with proper initial coin state $|\psi_0^-\rangle$ localization in the range $\phi \in (0, 3\pi/2)$, whereas with $|\psi_0^+\rangle$ exhibits localization in the range $\phi \in (\pi/2, 2\pi)$. The above numerical simulations show that there exists Anderson localization for 1D QW with phase disorder ϕ at origin depending on the value of ϕ and the initial coin state.

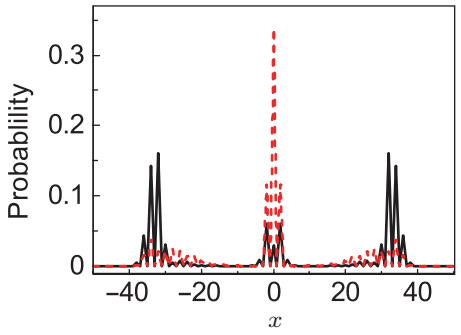


Fig. 5. The distributions of 1D Hadamard QWs with disorder of a single-phase defect $\phi = \pi/3$ in $x = 0$ after 50-step evolution for symmetric (solid line) and antisymmetric (dotted line) initial coin states.[45]

The explanation on the Anderson localization of 1D QW with the phase defect at origin is put forward in Ref. [45]. This method can also be used to explain the localization effect of QWs with other kinds of disorders. It is necessary to analyze the distribution property of the eigenstates of unitary operator. According to the application of U_ϕ, the amplitudes of the coin corresponding to walker at position $x = 0$ satisfy

$$\begin{aligned} \sqrt{2}\alpha_{-1}(t+1) &= w\alpha_0(t) + w\beta_0, \\ \sqrt{2}\beta_1(t+1) &= w\alpha_0(t) - w\beta_0, \end{aligned} \tag{12}$$

and the amplitudes corresponding to walker at position $x \neq 0$ satisfy

$$\begin{aligned} \sqrt{2}\alpha_x(t+1) &= \alpha_{x+1}(t) + \beta_{x+1}(t), \\ \sqrt{2}\beta_x(t+1) &= \alpha_{x-1}(t) - \beta_{x-1}(t), \end{aligned} \tag{13}$$

where $w = \mathrm{e}^{\mathrm{i}\phi}$ with $\phi \in (0, 2\pi)$. For the double-step operator U_ϕ^2, the amplitudes of the eigenstates take the time-independent form

$$2\lambda\alpha_0 = \alpha_2 + \beta_2 + w\alpha_0 - w\beta_0, \tag{14}$$

$$2\lambda\beta_0 = w\alpha_0 + w\beta_0 - \alpha_{-2} + \beta_{-2}, \tag{15}$$

$$2\lambda\alpha_{-2} = w\alpha_0 + w\beta_0 + \alpha_{-2} - \beta_{-2}, \tag{16}$$

$$2\lambda\beta_2 = \alpha_2 + \beta_2 - w\alpha_0 + w\beta_0, \tag{17}$$

and

$$2\lambda\alpha_{2x} = \alpha_{2x+2} + \beta_{2x+2} + \alpha_{2x} - \beta_{2x}, \quad x \neq 0, -2, \tag{18}$$

$$2\lambda\beta_{2x} = \alpha_{2x} + \beta_{2x} - \alpha_{2x-2} + \beta_{2x-2}, \quad x \neq 0, 2, \tag{19}$$

where λ is the eigenvalue of U_ϕ^2.

From Eqs. (18) and (19), we can obtain

$$\beta_{2x+2} = (\alpha_{2x+2} - \lambda\beta_{2x})/(\lambda - 1), \quad x \neq -2, 0. \tag{20}$$

By using Eq. (20) together with Eq. (19), one can obtain

$$\lambda\alpha_{2x+2} - 2(\lambda^2 - \lambda + 1)\alpha_{2x} + \lambda\alpha_{2x-2} = 0. \tag{21}$$

The general solution of the above equation is

$$\alpha_x = c_1 y^x + c_2 y^{-x}. \tag{22}$$

Here, y satisfies

$$\lambda y^2 - 2(\lambda^2 - \lambda + 1)y + \lambda = 0, \tag{23}$$

so does $1/y$. For $x \to \pm\infty$, the amplitude of the wavefunction must have $\alpha_x \to 0$ due to normalization. Therefor,

$$\begin{aligned} &\alpha_x = c_1 y^x, \quad x \geqslant 2, \\ &\alpha_x = c_2 y^x, \quad x \leqslant 2. \end{aligned} \tag{24}$$

Thus,

$$\begin{aligned} &\beta_x = c_1 \frac{y - \lambda}{\lambda - 1} y^{x-1}, \quad x \geqslant 2, \\ &\beta_x = c_2 \frac{1 - \lambda x}{\lambda - 1} y^{-x}, \quad x \leqslant -2. \end{aligned} \tag{25}$$

From Eqs. (14) and (17), one can obtain

$$\alpha_0 = 1/\lambda[\alpha_2 + \beta_2(1 - \lambda)]. \tag{26}$$

Substituting Eqs. (24) and (25) into Eq. (26), we have

$$\alpha_0 = c_1. \tag{27}$$

From Eqs. (15) and (16), we can obtain

$$\beta_0 = [\beta_{-2} + \alpha_{-2}(\lambda - 1)]/\lambda. \tag{28}$$

Thus, from Eqs. (23)–(25), we can obtain

$$\beta_0 = c_2 \frac{1 - \lambda x}{\lambda - 1}. \tag{29}$$

From Eqs. (14), (15), (24), and (25), we have

$$\begin{aligned} &w\beta_0 = c_1 \left(y + w - 2\lambda + \frac{y - \lambda}{\lambda - 1} \right), \\ &c_1 w = \beta_0 \left(2\lambda - y - w + y\frac{\lambda - 1}{1 - \lambda y} \right). \end{aligned} \tag{30}$$

From the above equation and Eq. (15), one can obtain

$$y_\pm = \frac{1}{2\cos(2\pi\phi) \mp 2\sin(2\pi\phi) - 3}. \tag{31}$$

From Eqs. (28)–(31), one can obtain

$$c_2 = c_1(w \mp \mathrm{i}w \pm \mathrm{i}). \tag{32}$$

Therefor, the amplitude of the localized stationary state is given by

$$\alpha_0^\pm = c_1, \quad \beta_0^\pm = \mp \mathrm{i}c_1, \tag{33}$$

and

$$\begin{aligned} &\alpha_x^{(\pm)} = c_1 y_\pm^x, \quad x \geqslant 2, \\ &\alpha_x^{(\pm)} = c_1(w \mp \mathrm{i}w \pm \mathrm{i}) y_\pm^{-x}, \quad x \leqslant -2, \\ &\beta_x^{(\pm)} = c_1(1 - w \mp \mathrm{i}w) y_\pm^x, \quad x \geqslant 2, \\ &\beta_x^{(\pm)} = \mp \mathrm{i}c_1 y_\pm^{-x}, \quad x \leqslant -2. \end{aligned} \tag{34}$$

Here, $c_1 = \sqrt{(1 + y_\pm)/2}$, and the $\pm$ sign of the results depends on the signs of $y_\pm$.

From the above analytic results, the eigenstates of U_ϕ^2 is obtained. Then the probability distribution of eigenstates can be obtained by doing partial trace out of the coin state. Some of the profiles of eigenstates exhibit allocation at origin, such eigenstates are called localized eigenstates. It turns out that the phase defect ϕ at origin results in the appearance of the localized eigenstate. The number of the localized stationary states depends on the value of ϕ. There is only one localized stationary state in the range $\phi \in (0, \pi/2] \cup [3\pi/2, 2\pi)$, while there are two such states in the range $\phi \in (\pi/2, 3\pi/2)$.

The initial state of the whole system is decomposed into the basis consisting of the eigenstates of unitary operator U_ϕ^2. If the decomposition of the initial state contains the localized eigenstate, QWs will exhibit Anderson localization. Thus, the overlap between the initial state and the localized eigenstates is defined to measure the lower bound for the probability of the existence of Anderson localization. The overlap F depends on the value ϕ of the phase disorder and the initial state as shown in Fig. 6. For the antisymmetric initial coin state $(|0\rangle - \mathrm{i}|1\rangle)/\sqrt{2}$, the overlap satisfies $F \gg 0$ for $\phi \in (0, 3\pi/2]$. Thus, one can observe the localization effect for the antisymmetric initial coin state with $\phi \in (0, 3\pi/2)$ in $x = 0$. Whereas for the asymmetric initial state $|0\rangle$ the overlap satisfies $F \gg 0$ for different range $\phi \in (\pi/2, 2\pi)$. Thus we can explain the reason why the localization effect depends on the value of the phase defect ϕ and the initial coin states.

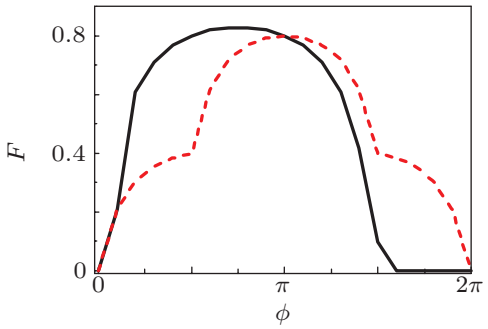


Fig. 6. The overlaps F between the initial states and localized eigenstates as a function of the value of phase defect ϕ. The solid black line corresponds to the initial coin state $(|0\rangle - \mathrm{i}|1\rangle)/\sqrt{2}$, the dashed red line corresponds to the initial coin state $|0\rangle$.[45]

It is necessary to satisfy two conditions to explain the exist of the localization effect. Firstly, there must be localized eigenstates of the unitary operation for 1D QWs with disorder. Secondly, the overlap between the localized eigenstates and the initial state of the whole system is much bigger than 0. If and only if both are satisfied, 1D QWs with disorder exhibit the localization effect. The properties of 1D QWs with a single-phase defect at other position $x \neq 0$ can be discussed in the similar way.

We have shown there exist the localization in QWs with static disorder at origin on the walker. Next we will show dynamical localization of QWs with proper position- or time-dependent disorders on the walker which is represented by variance changed quasi-periodically.

The properties of the 1D QWs with position-dependent phase disorders are studied and the explanation on the dynamical localization is investigated by analyzing the eigenstates and eigenvalues of the unitary operator of the evolution in Ref. [46]. The behavior of generalized QWs where the irrational phases ϕ are added depending on the position x is studied in detail. The unitary operator in this case is

$$U_{\phi(x)} = \left(\sum_c |c\rangle\langle c| \otimes S_{c\phi(x)}\right)(C \otimes I), \tag{35}$$

where $S_{c\phi(x)}|x\rangle = \mathrm{e}^{\mathrm{i}\phi(x)}|x+(-1)^c\rangle$ $(c = 0,1)$ and $\phi(x) = 2\pi xq/p$ with coprime q and p. This model predicts dynamical localization as shown in Fig. 7. Numerical simulations show that for large step t a ballistic diffusion occurs. The oscillation of standard deviation σ and the difference between σ for odd and even p can be seen. Oscillation of σ^2 are damped more quickly in the odd case than even case.

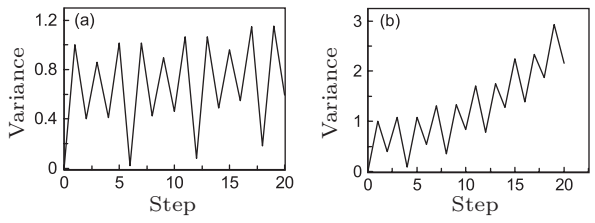


Fig. 7. Evolution of the variance σ^2 for $q = 1$, $p = 3$ (a), and $p = 4$ (b).

The properties of 1D stroboscopic QWs with time-dependent phase disorders are analyzed in Ref. [47]. In stroboscopic QWs, the walker walks in the space consisting of eigenstates of the Hamiltonian H with $H|n\rangle = E_n|n\rangle$. The walker acquires a relative phase depending on the time interval between each two steps. The unitary operator of one step for stroboscopic QWs is

$$U_{\mathrm{s}} = \left(\sum_c |c\rangle\langle c| \otimes S_{\mathrm{c}}\right)\left(C \otimes \mathrm{e}^{-\mathrm{i}H\tau/\hbar}\right), \tag{36}$$

where τ is the interval time between two steps. The smallest possible time interval is given by $T = 2\pi\hbar\lambda/(E_n - E_{n+2})$. The dynamic of the stroboscopic QWs shows the non-classical property dynamical localization in Fig. 8, i.e., the quantum walker spreads more slowly than the classical walker to linear diffusion when τ is not a rational multiple of the Talbot time as shown in Fig. 8. The system exhibits high-order quantum resonances and the close link to nonlinear δ-kicked system in quantum chaos theory, thus QW can be useful for modeling quantum chaos.

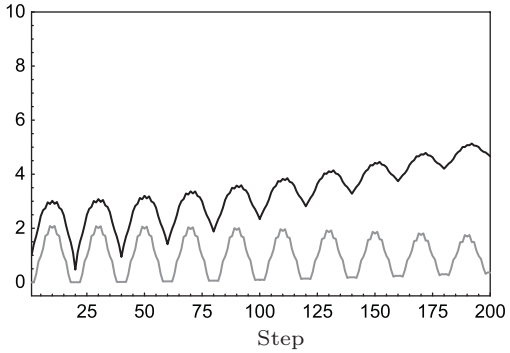


Fig. 8. Standard deviation σ (black curves) and mean $\langle n\rangle$ (grey curves) for stroboscopic Hadamard walks with $\tau = T/10$.[47]

3.2. QWs with disorder on the coin

There exist localization in 1D QW with time- or position-dependent phase disorder added on the walker as described in the previous part. Anderson localization effect can also be observed by choosing other forms of disorders on the quantum coin.

Disorders added on the coin can also be in spatial, temporal and spatio–temporal forms and induce the change in interference pattern.[48] The one step time evolution operation for QWs with spatial disorder is

$$U_{\mathrm{SD}} = S[C_{\mathrm{SD}}(\widetilde{\theta}_x) \otimes I], \tag{37}$$

where $C_{\mathrm{SD}}(\widetilde{\theta}_x)$ is the position-dependent coin operation. Spatial disorder can be added on the coin by making a position-dependent coin operation with different values of $\theta_x \in (0,\pi)$ chosen for each position x. For example, the spatial disorder added on the coin operations which is dependent on the walker's position can be described as

$$C_{\mathrm{SD}} = \sum_x |x\rangle\langle x| \begin{pmatrix} \cos(\theta x) & -\sin(\theta x) \\ \sin(\theta x) & \cos(\theta x) \end{pmatrix}. \tag{38}$$

The properties of 1D QWs with spatial inhomogeneous disorder are discussed analytically in Ref. [49]. The analytical solution shows that the limit distribution of QWs with inhomogeneous coin operation divided by any power of time is localized at origin when the inverse period of coins is irrational number. In this case, the coin operator at each position is different from the others. QWs with spatial inhomogeneous coin flipping are localized at the origin position. Temporal disorder $\theta_t \in (0,\pi)$ is randomly assigning different coin operation for each step of the QWs, thus the evolution operator is

$$U_{\mathrm{TD}} = U_x(\theta_t)\cdots U_x(\theta_3)U_x(\theta_2)U_x(\theta_1). \tag{39}$$

Spatio–temporal disorder is randomly assigning different coin operation for each position and each step. The evolution operator of QWs with Spatio-temporal disorder is

$$U_{\mathrm{S-TD}} = U_x(\theta_{x,t})\cdots U_x(\theta_{x,3})U_x(\theta_{x,2})U_x(\theta_{x,1}). \tag{40}$$

The distributions after 100 steps with ratio $4/5$ Hadamard coin operation ($\theta = \pi/4$) and ratio $1/5$ spatial, temporal and spatio-temporal disorder are shown in Fig. 1(a) of Ref. [48]. The trend of localization is shown even with a small percentage of disorder. In Fig. 1(b) of Ref. [48] the distributions are shown for the coin operations are randomly chosen for the complete evolution. The impact of spatial disorder on the localization is stronger compared with that of the temporal disorder and spatio–temporal disorder.

Figure 2(a) of Ref. [48] shows standard deviation as a function of step for 1D standard QWs and QWs with spatial, temporal, and spatio–temporal disordered coin operation. Figure 2(b) of Ref. [48] shows a sudden decrease in standard deviation even for small increase in percentage of disorder and the impact of spatial disorder is stronger than other forms of disorder.

QWs with three different forms of disorder added on the coin are studied extensively. The interference pattern is changed due to the disorder and entanglement is generated during the evolution of QWs. The impact of disorder on the entanglement between the particle and position space measured by von Neaumann entropy is shown in Fig. 3(a) of Ref. [48]. The degree of entanglement as a function of the ratio of disorder for standard QWs and QWs with three different forms of disorder is shown in Fig. 3(b). Degree of entanglement as a function of time is directly proportional to the size of the position space. Spatial disorder suppresses the degree of entanglement, whereas temporal and spatio–temporal disorder enhances the entanglement. This opens up an important question what is the interplay between the disorder and entanglement.

Dynamic localization can also be observed in 1D QWs by assigning randomly a different set of coin operators for each step of the walk. The unitary operator is $U_{\mathrm{c}}(\phi) = S(C_{\mathrm{B}} \otimes I)$, where C_{B} is the coin operator described as

$$C_{\mathrm{B}} = \begin{pmatrix} \mathrm{e}^{\mathrm{i}\xi}\cos\theta & \mathrm{e}^{\mathrm{i}\zeta}\sin\theta \\ \mathrm{e}^{-\mathrm{i}\zeta}\sin\theta & -\mathrm{e}^{\mathrm{i}\xi}\cos\theta \end{pmatrix}. \tag{41}$$

With $\xi = \zeta = 0$, C_{B} is the unbiased Hadamard coin operation. Evolution of QWs with disordered coin operation is realized by choosing different coin operation for each step from a set of operators in the $U(2)$ group. The evolution is still unitary and leads to interference of amplitudes of the walker. By choosing the proper range of the parameters, the walker can be strongly localized as shown in Fig. 9. The ultracold atoms in an optical lattice offer opportunities to implement this kind of disordered QWs, which is unitary and induces localization.[50] The position distribution of QWs with disordered coin operation after 100 steps is shown in Fig. 9 when different θ is randomly picked for each step from subsets $\theta_1 \in (0,\pi/4]$ and $\theta_2 \in (\pi/4,\pi/2]$ for $C_{\mathrm{B}}(\xi,\zeta,\theta_1)$ and $C_{\mathrm{B}}(\xi,\zeta,\theta_2)$, respectively. Other parameters are picked from the range $\xi,\zeta \in (0,\pi/2]$. The parameters for each random coin operation in the evolution are generated from a random number generator program with equal probabilities of any number in the specific range. QWs with $C_{\mathrm{B}}(\xi,\zeta,\theta_1)$ diffuse and the position distribution does not show sharp peaks while that of the standard QWs with identical Hadamard coin operation exhibit two sharp peaks. QWs with $C_{\mathrm{B}}(\xi,\zeta,\theta_2)$ behave localization around the origin.

Besides 1D QWs, one can observe localization in the extended multi-degree QWs.[27] For instance, in 2D QWs with Grover coin operator exhibit localization,[51] and localization phenomenon is observed in 1D QWs with two entangled coins.[52] Compared with the standard QWs whose coin operator has two freedom degrees, three-state QWs whose coin has three sides also exhibit localization.[53] The eigenvalues and eigenvectors can be calculated and it is shown that the localization depends on the degeneration of eigenvalues of the unitary operator and the initial state of the system.

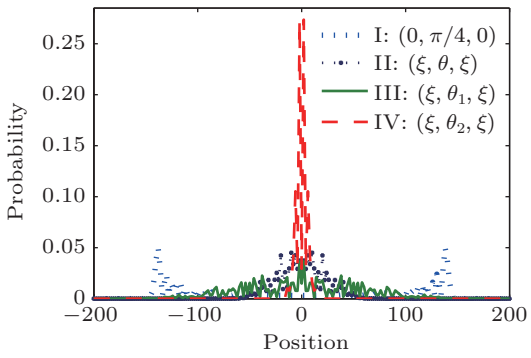


Fig. 9. Comparison of the probability distribution of the QWs evolve by picking different coin operator parameter with initial state $(|0\rangle + \mathrm{i}|1\rangle)/\sqrt{2}$. Curve I: Hadamard walk ($\theta = \pi/4$), curve II: $\xi,\theta,\zeta \in (0,\pi/2)$, curve III: $\xi,\zeta \in (0,\pi/2)$ and $\theta \in (0,\pi/4)$, and curve IV: $\xi,\zeta \in (0,\pi/2)$ and $\theta \in (\pi/4,\pi/2)$.[50]

4. The impact of decoherence on QWs

Decoherence plays the role of transforming QWs to RWs. Besides reducing quantum coherence, decoherence can provide a method to tune QWs to improve their algorithm properties. The evolution of QWs with decoherence is usually non-unitary, thus the density operators ρ are needed for describing mixed states. The pure state satisfies $\rho^2 = \rho$. For non-unitary QWs, the extra non-unitary operation is added,

$$\rho(t+1) = (1-p)U\rho U^{\dagger} + p\sum \mathbb{P}_j U\rho(t)U^{\dagger}\mathbb{P}_j^{\dagger}, \qquad (42)$$

where $U = \left(\sum_c |c\rangle\langle c| \otimes S_c\right)(C \otimes I)$ is the unitary operator for QWs without decoherence, $\mathbb{P}_j$ is an extra non-unitary operator depending on what sort of decoherence we are considering and satisfy

$$\sum_j \mathbb{P}_j^{\dagger}\mathbb{P}_j = I, \qquad (43)$$

and p is the probability of decoherence of each step. With different kind of decoherence, we can replace the coin or the conditional shift operator by non-unitary operator. We briefly review the properties of QWs with decoherence through analyzing the above equation for decoherence on the coin, the walker, or both coin and walker.

We introduce the decoherence induced by measurements which are independently in each step. In this case, $\mathbb{P}_j$ is the action of decoherence induced by measurement projection. Simulations for QWs with decoherence induced by the measurements on the coin, on the walker, or on both coin and walker have been shown by Kendom *et al.*[55]

In order to show the impact of decoherence induced by measurement on the behavior of QWs on the line, the standard deviation as a function of the decoherence rate p is calculated. From Fig. 11, one can know that the variance decay from the quantum to classical with nearly the same tendency for three forms of decoherence, i.e., decoherence on the coin, the walker or both coin and walker. The results meet the fact that quantum states are fragile with decoherence. The distribution of QWs with decoherence is shown in Fig. 10. There exists a top-hat distribution for decoherence on the walker with the rate $p = 0.03$, while the top-hat distribution does not occur in the case of decoherence on the coin. The property of top-hat distribution is useful for computational physicists because it can provide uniform sampling over a specific range. It is shown that the optimal top-hat appears when all the quantum correlations are removed after steps.[56] Thus, decoherence can reduce the quantum behavior in QWs, and low decoherence may be useful in practice. We have reviewed the results of the impact of decoherence on the coin, on the walker or on both coin and walker induced by measurement for 1D QWs . In this review, we consider analytically the decoherence on the coin in detail.[14,59] If the quantum coin is measured after each step, then the QWs are reduced to RWs. The quantum effect in QWs can also be reduced by replacing the same coin with a new coin for each step.[14,57] The two approaches are equivalent in the classical limit. We take the solution of QWs on a line with a single coin subject to decoherence which is induced by dephasing as an example.

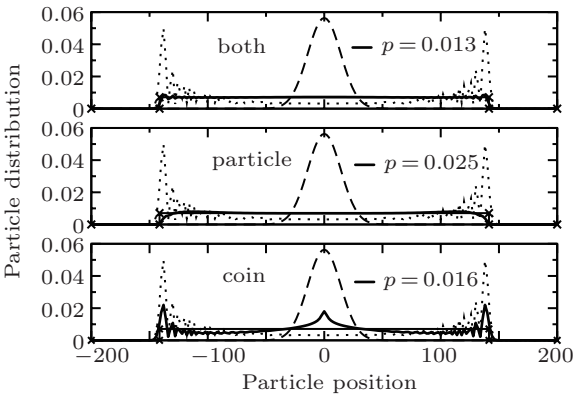


Fig. 10. Distribution of the position for QWs on a line after 200 steps. Pure quantum (dotted), fully classical (dashed), and with decoherence (solid).[55]

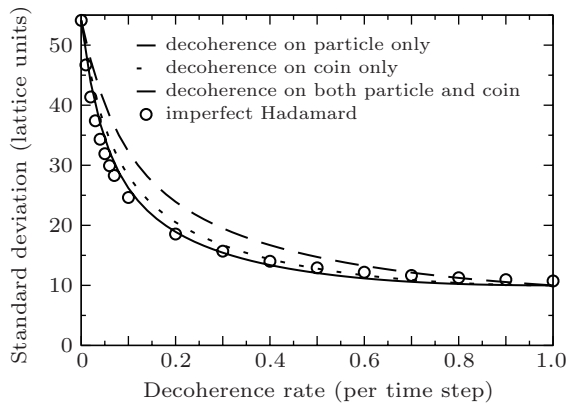


Fig. 11. Standard deviation of the position on a line for different models of decoherence.[55]

We introduce the analytical method of Fourier transformation to solve the system of QWs with decoherence on the coin. The shift operator is given by $S|x,c\rangle = |x+c,c\rangle$, where x is the walker's position and c is the state of the coin. Transform from the position basis $|x\rangle$ to the Fourier basis $|k\rangle$ is expressed as

$$|k,c\rangle = \sum_x \mathrm{e}^{\mathrm{i}kx}|k,c\rangle. \qquad (44)$$

It is found that

$$U|x,c\rangle = C_k|k,c\rangle, \qquad (45)$$

where C_k acts on the coin

$$C_k = \frac{1}{\sqrt{2}}\begin{pmatrix} \mathrm{e}^{\mathrm{i}k} & \mathrm{e}^{\mathrm{i}k} \\ \mathrm{e}^{-\mathrm{i}k} & -\mathrm{e}^{-\mathrm{i}k} \end{pmatrix}. \qquad (46)$$

The walker is at the origin and the coin is in the state ψ, thus the initial state can be expressed as

$$\rho_0 = |0,\psi_0\rangle\langle 0,\psi_0|$$

$$= \int \frac{\mathrm{d}k}{2\pi} \int \frac{\mathrm{d}k'}{2\pi} |k\rangle\langle k'| \otimes |\psi_0\rangle\langle\psi_0|. \quad (47)$$

The non-unitary evolution of QWs with decoherence is written as

$$\rho_t = \int \frac{\mathrm{d}k}{2\pi} \int \frac{\mathrm{d}k'}{2\pi} |k\rangle\langle k'| \otimes \mathbb{P}^t_{kk'} |\psi_0\rangle\langle\psi_0|, \quad (48)$$

with

$$\mathbb{P}_{kk'} |\psi_0\rangle\langle\psi_0| = \sum_{j=\pm} \mathbb{P}_j C_k |\psi_0\rangle\langle\psi_0| C_{k'} \mathbb{P}_j^{\dagger}, \quad (49)$$

where the set of projector $\mathbb{P}_\pm$ is the decoherence acting on the coin with the form of

$$\mathbb{P}_\pm = \frac{1}{\sqrt{2}} \begin{pmatrix} \mathrm{e}^{\pm \mathrm{i}\chi} & 0 \\ 0 & \mathrm{e}^{\mp \mathrm{i}\chi} \end{pmatrix}, \quad (50)$$

where the value of χ represents the strength of dephasing. $\chi = 0$ ($p = 0$) and $\chi = \pi/4$ ($p = 1$) correspond to the pure QWs without decoherence and the complete classical RWs, respectively. It is difficult to calculate the state of the system ρ explicitly. However, the property of QWs can be given by the moment which shows how fast the walker spreads, i.e.,

$$\begin{aligned} \langle x^m \rangle &= \sum_x x^m P(x,t) \\ &= \sum_x x^m \int \frac{\mathrm{d}k}{2\pi} \int \frac{\mathrm{d}k'}{2\pi} \langle x|k\rangle \langle k'|x\rangle \\ &\quad \times \mathrm{Tr_c} \left(\mathbb{P}_k k'^t |\psi_0\rangle\langle\psi_0| \right). \end{aligned} \quad (51)$$

The variance $\langle x^2 \rangle - \langle x \rangle^2$ can be analytically calculated in the limit large t

$$\langle x^2 \rangle - \langle x \rangle^2 \simeq t(\cot^2 2\chi + \csc^2 2\chi) + O(1). \quad (52)$$

The analytical results of variance for QWs with dephasing on the coin show that even a small amount of decoherence can make the QWs become RWs. The comparison between the numerical results and analytical results is shown in Fig. 12. The variance of numerical simulation matches the analytical result. The variance changes linearly with t and the rate of growth approaches 1 with increasing decoherence at long t. The inset figure shows that the dependence of variance at short t exhibits quadratic growth.

Variance can be solved analytically for QWs with decoherence, whereas it is different to calculate the position distribution $P(x,t)$ analytically. Thus, it is straightforward to solve $P(x,t)$ of QWs with decoherence numerically by using quantum trajectory techniques. Figure 13 shows the position distribution changes from the standard QWs to classical RWs by choosing the same initial coin state $|1\rangle$. The signs of interference which include the peak at $t/\sqrt{(2)}$ and the oscillations

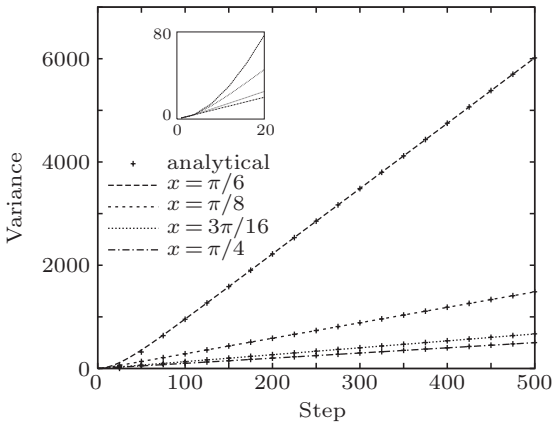


Fig. 12. Variance versus step t with decoherence for $\chi = \pi/16, \pi/8, 3\pi/16, \pi/4$.[59]

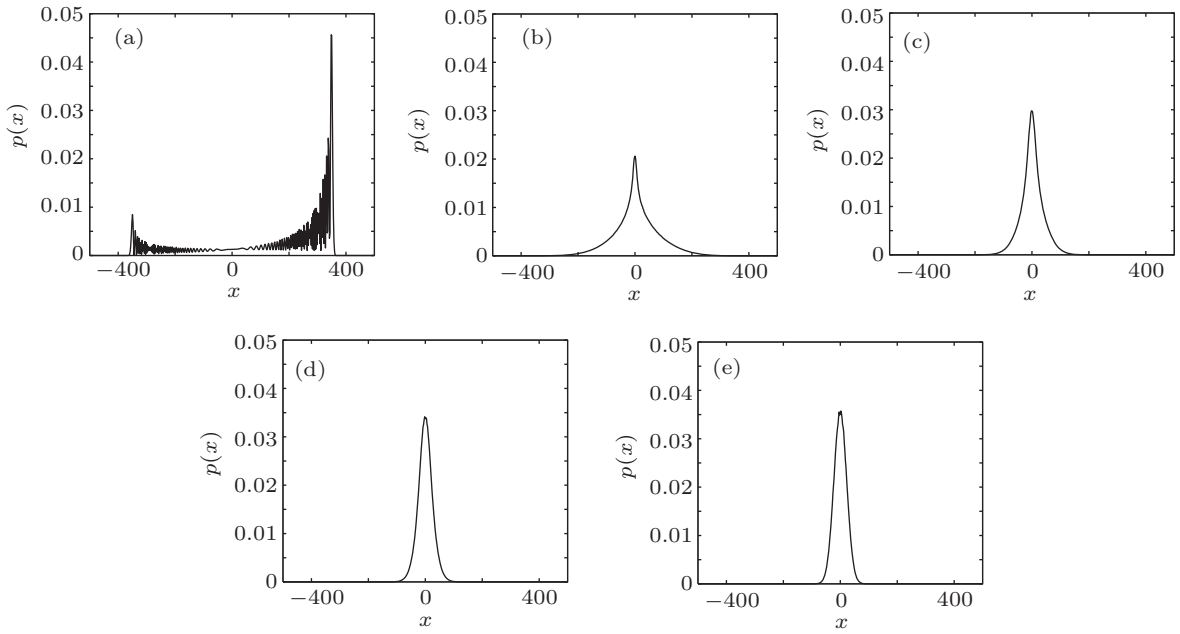


Fig. 13. The position distribution after $t = 500$ for QWs with decoherence: (a) $\chi = 0$ (unitary case), (b) $\chi = \pi/16$, (c) $\chi = \pi/8$, (d) $\chi = 3\pi/16$, and (e) $\chi = \pi/4$.[59]

in distribution disappear quickly with the presence of decoherence. For QWs with decoherence, the peak at $x = 0$ appears in the distribution. However, the peak is broadened compared to the classical. When decoherence parameter $\chi = \pi/4$, the distribution is binomial. For QWs without decoherence, the evolution of the system is unitary and the interference effects cause the initial state to have impact on the evolution. The presence of decoherence eliminates the interference effect and the initial state nearly has no impact on the evolution after a short time t.

Decoherence on the coin of QWs can be in the time-dependent way which makes QWs transfer between classical and quantum behavior by controlling the decoherence of coin.[58] Prior to each unitary coin operation, a complete-positive trace-preserving map is applied to the coin. The map is described as

$$\varepsilon\rho_{\rm c} = \sum_{n\in 0,\pm} A_n \rho_{\rm c} A_{\rm c}^{\dagger}, \tag{53}$$

with

$$\sum_{n\in(0,\pm)} A_n^{\dagger} A_n = I, \tag{54}$$

and

$$A_0 = \sqrt{\kappa(t)}I, \quad A_{\pm} = \sqrt{1-\kappa(t)}P^{\pm}, \tag{55}$$

where $P^{\pm} = \langle\pm|\pm\rangle$ and $\kappa(t)$ is the step-dependent strength of the measurement. The periodic dynamical map is introduced as

$$\kappa(t) = \cos\eta t. \tag{56}$$

Driving the coin with period $\kappa(t) = \cos t/10$ affects variance as shown in Fig. 14(a). variance oscillates periodically between classical diffusive and quantum ballistic values at various time. Figures 14(b)–14(d) show numerical results for the position distribution as a mixture of classical and quantum distributions ($t = 22$), nearly fully quantum ($t = 32$) and nearly fully classical ($t = 48$). The variances for a periodic driving field with two other higher frequencies are shown for $\kappa(t) = \cos t/2$ (see Fig. 15(a)) and $\kappa(t) = \cos 3t/10$ (see Fig. 15(b)). The periodicity of the variance versus time commensurate with the periodicity observed for the sinusoidal driving function. Thus the QWs with driven coin exhibit the oscillation between RWs and QWs.

In summary, QWs with decoherence on the coin has been solved analytically and shows us the transition from QWs to RWs. QWs with decoherence on the walker have also been analyzed in details in Ref. [60]. As the decoherence for moderate timescale the quantum effect persist, while to a point of critical damping, QWs is reduced to RWs. If the quantum effect persists, the useful algorithmic properties are better than standard QWs. Thus decoherence in QWs have potential algorithm application for quantum computing.

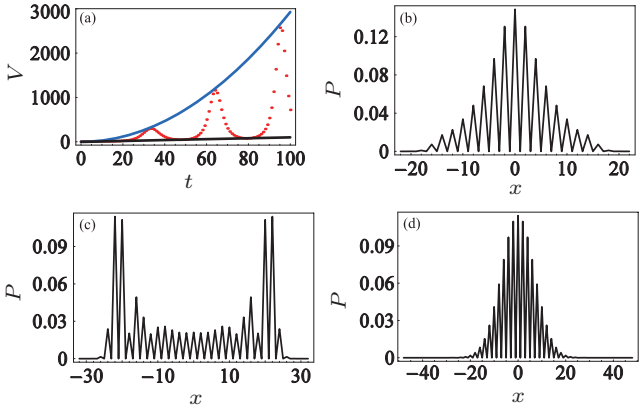


Fig. 14. (a) Variance as a function of t with initial state $|0\rangle(|+\rangle + i|-\rangle)/\sqrt{2}$: unitary evolution (blue solid), driving with $\kappa(t) = \cos t/10$ (red dot), and RWs (black solid). (b)–(d) Position distribution P after (b) 22, (c) 32 and (d) 48 steps.[58]

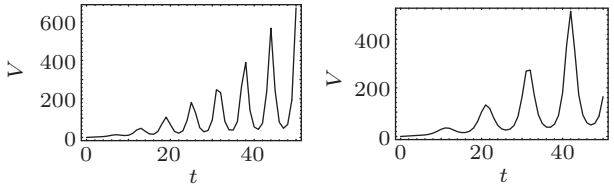


Fig. 15. Variance vs step of QWs driving with (a) $\kappa(t) = \cos t/2$ and (b) $\kappa(t) = \cos 3t/10$.[58]

5. Experiments of quantum walks

As QWs have many potential applications, a host of physical systems have been used to implement QWs experimentally, such as trapped atoms,[61,62] trapped ions,[31,63] nuclear magnetic resonance (NMR) systems,[64] and photonic quantum systems, mainly including bulk optics,[17,65] waveguide structures,[15,40,43,66–69] and fiber loop networks,[38,39,41] which are concentrated on in this section of this Review. Photons can spread in free space at the speed of light without low temperature and vacuum conditions. The polarization quantum bit of photons mostly used in experiments can be easily manipulated. Photons can also provide path or angular momentum as quantum bits. Besides, photonic quantum systems are robust since photons do not easily interact with each other, and photonic quantum systems will be scalable in the near future.[70]

White *et al*. realized discrete single-photon QWs in space via bulk optics in 2010.[65] Figure 16(a) is their experimental schematic. They choose single photons as the walker and two orthogonal polarization states of photons, horizontal and vertical, to represent the coin. The coin operator is realized with half-wave plates. The beam displacer, which is the key component of the bulk optics scheme, is birefringent calcite and properly cut to let light with vertical polarization through and light with horizontal polarization acquire a lateral displacement into a neighboring spatial mode, thus realizing the step operator of QWs. The initial state of the QW is prepared with a half-wave plate and a quarter-wave plate set to suitable angles against the optical axis and the input photons transverse

a half-wave plate and a beam displacer for each step. Photons get into different spatial modes after each step and these spatial modes constitute the lattice sites of the QWs, which are labeled as shown in Fig. 16(b). They measured the probability distribution of the QW with up to 6 steps and by introducing tunable decoherence, which is achieved by tilting the beam displacer(see Fig. 16(c)), the quantum-to-classical transition is then observed. In 2012, using similar experimental setups of bulk optics, White *et al*. successfully observed topologically protected bound states in photonic quantum walks.[17]

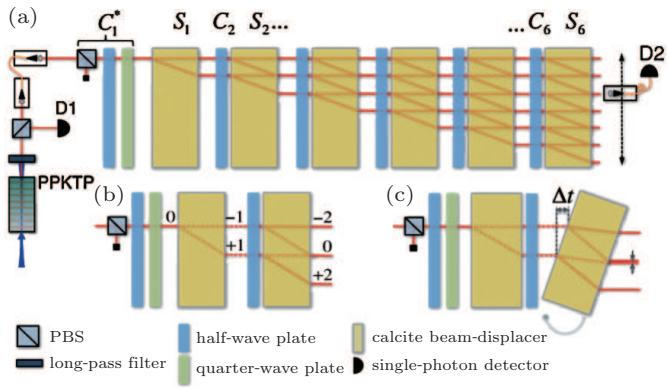


Fig. 16. Experimental schematic of Ref. [65].

Compared with bulk optics systems, physical systems with waveguide structures seem to be a more promising platform for the study of QWs. A quantum walk of a two-photon polarization-entangled state was experimentally simulated via integrated waveguide circuits in a recent literature and therein Anderson localization was observed with certain position dependent disorder.[15] Figure 17 is the experimental schematic. The showed waveguide structure is actually equivalent to a cascade of balanced beam splitters (BSs) laid up in a Mach–Zehnder (MZ) interferometers array. Each directional coupler represents a BS, which is independent of polarization. Photons generated from spontaneous parametric down-conversion were chosen to be the walker and its two possible propagating paths through a BS to be the internal coin. Thus, each

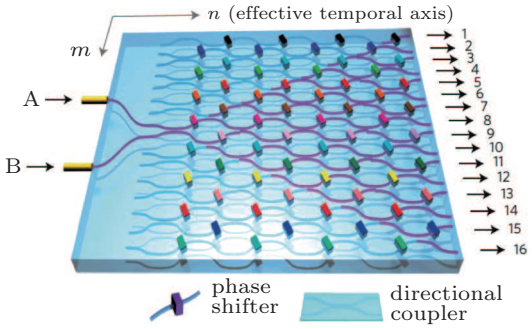


Fig. 17. Integrated circuit for disordered QW. Scheme of the network of directional couplers implementing an eight-step one-dimensional QW with static disorder. Different colors indicate different phase shifts and violet waveguides represent the accessible paths for photons injected from inputs A and B.[15]

directional coupler serves as the coin operation as well as the step operator at the same time for each step. Besides, phase shifters were added at each directional coupler's output port before the next one's input port in order to have Anderson localization phenomenon and were implemented by deforming one of the S-bend waveguides at the output of each directional coupler, aiming to make a different between the two output optical paths. The waveguide circuits were constructed by taking advantage of femtosecond laser writing technology. Finally, the QW was realized up to 8 steps and the evolution towards Anderson localization was observed in real time.

Unlike the former two physical systems referred above, the QWs realized in which proceed in space, optical fiber loop networks can realize QWs in time. In 2010, Silberhorn *et al*. presented a coined quantum walk on line up to 5 steps, using a fiber loop network.[38] Figure 18 is the sketch of the setup. Photons obtained by attenuating a pulsed laser source were used as the walker and its polarization as the coin. A combination of a half-wave plate and a quarter-wave plate was employed to generate the desired initial state and another half-wave plate was used to do the coin flipping. After that, photons reach PBS1 and the horizontal and vertical components are separated spatially into two polarization-maintaining fiber with different lengths so that the two components are separated in time, equaling taking a step in time. Then, the two paths recombines to one at PBS2 to continue propagating in the fiber loop to the next step. In 2011, Silberhorn *et al*. pushed the one-dimensional QW to 28 steps, using the similar fiber loop setup,[39] and in the next year, they developed the existing scheme of fiber loop network to implement a two-dimensional QW over 12 steps and 169 positions.[41]

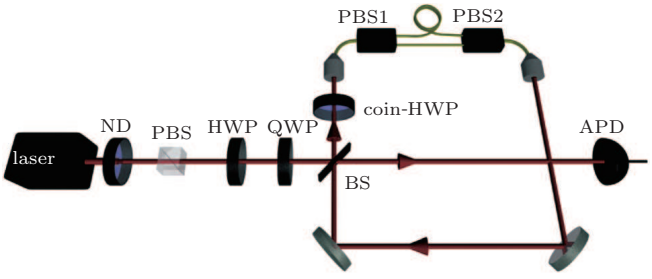


Fig. 18. Sketch of the setup. A laser field is attenuated to the single-photon level via neutral density filters (ND) and coupled into the network loop through a 50:50 beam splitter (BS). HWP: half-wave plate; QWP: quarter-wave plate; PBS: polarizing BS; APD: avalanche photodiode.[38]

In summary, QWs with pure quantum evolution tend to a ballistic spread while with decoherence introduced into, the walks undergo the transition from ballistic quantum walks to diffusive classical random walks. Besides, the impact of static disorder on QWs leads to localization phenomenon.

6. Conclusion

We have reviewed on the main ideas of discrete-time QWs and the impact of disorder and decoherence. There exists the localization in QWs with static disorder on the quantum walker or the coin, whereas the controllable decoherence can reduce the quantumness in QWs and transmit QWs to classical RWs.

References

[1] Feynman R P, Leighton R B and Sands M 1964 *Feynman Lectures on Physcis*
[2] Aharonov Y, Davidovich L and Zagury N 1993 *Phys. Rev. A* **48** 1687
[3] Farhi E and Gutmann S 1998 *Phys. Rev. A* **58** 915
[4] Ambainis A 2003 *International Journal of Quantum Information* **1** 507
[5] Childs A M, Cleve R, Deotto E, Farhi E, Gutmann S and Spielman D A 2003 35*th ACM Symposium on Theory of Computing* pp. 59–68
[6] Shenvi N, Kempe J and Whaley K B 2002 *Phys. Rev. A* **67** 052307
[7] Kempe J 2003 *Contemp. Phys.* **44** 307
[8] Childs M A 2009 *Phys. Rev. Lett.* **102** 180501
[9] Childs A M, Gosset D and Webb Z 2013 *Science* **339** 791
[10] Lovett N B, Cooper Everitt S M, Trevers M and Kendon V 2010 *Phys. Rev. A* **81** 042330
[11] Kendon V and Maloyer O 2007 *Theor. Comput. Sci.* **394** 187
[12] Kurzyński P and Wójcik A 2011 *Phys. Rev. A* **83** 062315
[13] Oliveira A C, Portugal R and Donangelo R 2006 *Phys. Rev. A* **74** 012312
[14] Brun T A, Carteret H A and Ambainis A 2003 *Phys. Rev. Lett.* **91** 130602
[15] Crespi A, Osellame R, Ramponi R, Giovannetti V, Fazio R, Sansoni L, Nicol F D, Sciarrino F and Mataloni P 2013 *Nat. Photon.* **7** 322
[16] Kitagawa T, Rudner M S, Berg E and Demler E 2010 *Phys. Rev. A* **82** 033429
[17] Kitagawa T, Broome M A, Fedrizzi A, Rudner M S, Berg E, Kassal I, Aspuru-Guzik A, Demler E and White A G 2012 *Nat. Commun.* **3** 882
[18] Xue P and Sanders B C 2008 *New J. Phys.* **8** 053025
[19] Xue P, Sanders B C and Leibfried D 2009 *Phys. Rev. Lett.* **103** 183602
[20] Xue P, Sanders B C, Blais A and Lalumiére K 2008 *Phys. Rev. A* **78** 042334
[21] Xu Y Y, Zhou F, Chen L, Xie Y, Xue P and Feng M 2012 *Chin. Phys. B* **21** 040304
[22] Xue P 2013 *J. Comput. Theor. Nanosci.* **10** 1606
[23] Aharonov D, Ambainis A, Kemp J and Vazitani U 2001 *Proc.* 33*rd Annual ACM STOC. ACM* NY 50
[24] Konno N 2002 *Quantum Inf. Process.* **1** 345
[25] Konno N 2005 *J. Math. Jpn* **57** 1179
[26] Kendon V M and Sanders B C 2004 *Phys. Rev. A* **71** 022307
[27] Mackay T D, Bartlett S D, Stephenson L T and Sanders B C 2002 *J. Phys. A: Math. Gen.* **35** 2745
[28] Du J, Li H, Xu X, Shi M, Wu J, Zhou X and Han R 2003 *Phys. Rev. A* **67** 042316
[29] Ryan C A, Laforest M, Boileau J C and Laflamme R 2005 *Phys. Rev. A* **72** 062317
[30] Lu D, Zhu J, Zou P, Peng X, Yu Y, Zhang S, Chen Q and Du J 2010 *Phys. Rev. A* **81** 022308
[31] Zähringer F, Kirchmair G, Gerritsma R, Solano E, Blatt R and Roos C F 2010 *Phys. Rev. Lett.* **104** 100503
[32] Schmitz H, Matjeschk R, Schneider Ch, Glueckert J, Enderlein M, Huber T and Schaetz T 2009 *Phys. Rev. Lett.* **103** 090504
[33] Cote R, Russell A, Eyler E E and Gould P L 2006 *New J. Phys.* **8** 156
[34] Karski M, Förster L, Choi J, Steffen A, Alt W, Meschede D and Widera A 2009 *Science* **325** 5937
[35] Do B, Stohler M L, Balasubramanian S, Elliott D S, Eash C, Fischbach E, Fischbach M A, Mills A and Zwickl B 2005 *J. Opt. Soc. Am. B* **22** 499
[36] Broome M A, Fedrizzi A, Lanyon B P, Kassal I, Guzik A A and White A G 2010 *Phys. Rev. Lett.* **104** 153602
[37] Kitagawa T, Broome M A, Fedrizzi A, Rudner M S, Berg E, Kassal I, Aspuru-Guzik A, Demler E and White A G 2012 *Nat. Commun.* **3** 882
[38] Schreiber A, Cassemiro K N, Potoček V, Gábris A, Mosley P J, Andersson E, Jex I and Silberhorn Ch 2010 *Phys. Rev. Lett.* **104** 050502
[39] Schreiber1 A, Cassemiro K N, Potoček V, Gábris A, Jex I and Silberhorn Ch 2011 *Phys. Rev. Lett.* **106** 180403
[40] Peruzzo A, Lobino M, Matthews J C F, Matsuda N, Politi A, Poulios K, Zhou X, Lahini Y, Ismail N, Wörhoff K, Bromberg Y, Silberberg Y, Thompson M G and O'Brien J L 2010 *Science* **329** 1500
[41] Schreiber A, Gábris A, Rohde P P, Laiho K, Štefaňák M, Potoček V, Hamilton C, Jex I and Silberhorn Ch 2012 *Science* **336** 55
[42] Crespi A, Osellame R, Ramponi R, Giovannetti V, Fazio R, Sansoni L, Nicola F D, Sciarrino F and Mataloni P 2013 *Nat. Photon.* **7** 322
[43] Owens J O, Broome M A, Biggerstaff D N, Goggin M E, Fedrizzi A, Linjordet T, Ams M, Marshall G D, Twamley J, Withford M J and White A G 2011 *New J. Phys.* **13** 075003
[44] Anderson P W 1958 *Phys. Rev.* **109** 1492
[45] Wójcik A, Luczak T, Kurzyński P, Grudka A, Gdala T and Bzdega M B 2012 *Phys. Rev. A* **85** 012329
[46] Wójcik A, Luczak T, Kurzyński P, Grudka A and Bednarska M 2004 *Phys. Rev. Lett.* **93** 180601
[47] Buerschaper O and Burnett K 2004 arXiv:0406039v2 [quant-ph]
[48] Chandrashekar C M 2012 arXiv:1212.5984v1
[49] Shikano Y and Katsura H 2010 *Phys. Rev. E* **82** 031122
[50] Chandrashekar C M 2011 *Phys. Rev. A* **83** 022320
[51] Inui N and Konishi Y 2004 *Phys. Rev. A* **69** 052323
[52] Liu Ch and Petulante N 2009 *Phys. Rev. A* **79** 032312
[53] Kollár B, Štefaňák M, Kiss T and Jex I 2010 *Phys. Rev. A* **82** 012303
[54] Souza A M and Andrade R F S 2013 *Science Reports* **3** 1976
[55] Kendon V and Tregenna B 2003 *Phys. Rev. A* **67** 042315
[56] Maloyer O and Kendon V 2007 *New J. Phys.* **9** 87
[57] Brun T A, Carteret H A and Ambainis A 2003 *Phys. Rev. A* **67** 052317
[58] Xue P and Sanders B C 2013 *Phys. Rev. A* **87** 022334
[59] Brun T A, Carteret H A and Ambainis A 2003 *Phys. Rev. A* **67** 032304
[60] Xue P and Zhang Y S 2013 *Chin. Phys. B* **22** 070302
[61] Karski M, Forster L, Choi J M, Steffen A, Alt W, Meschede D and Widera A 2009 *Science* **325** 174
[62] Genske M, Alt W, Steffen A, Werner A H, Werner R F, Meschede D and Alberti A 2013 *Phys. Rev. Lett.* **110** 190601
[63] Schmitz H, Matjeschk R, Schneider Ch, Glueckert J, Enderlein M, Huber T and Schaetz T 2009 *Phys. Rev. Lett.* **103** 090504
[64] Ryan C A, Laforest M, Boileau J C and Laflamme R 2005 *Phys. Rev. A* **72** 062317
[65] Broome M A, Fedrizzi A, Lanyon B P, Kassal I, Aspuru-Guzik A and White A G 2010 *Phys. Rev. Lett.* **104** 153602
[66] Perets H B, Lahini Y, Pozzi F, Sorel M, Morandotti R and Silberberg Y 2008 *Phys. Rev. Lett.* **100** 170506
[67] Sansoni L, Sciarrino F, Vallone G, Mataloni P, Crespi A, Ramponi R and Osellame R 2012 *Phys. Rev. Lett.* **108** 010502
[68] Solntsev A S, Sukhorukov A A, Neshev D N and Kivshar Y S 2012 *Phys. Rev. Lett.* **108** 023601
[69] Poulios K, Keil R, Fry D, Meinecke J D A, Matthews J C F, Politi A, Lobino M, Grafe M, Heinrich M, Nolte S, Szameit A and O'Brien J L 2013 arXiv:1308.2554v1
[70] Aspuru-Guzik A and Walther P 2012 *Nat. Phys.* **8** 285